8 Multi-dimensional diagnostics in space and time

Clemens F. Kaminski and Marshall B. Long

8.1 Introduction

The coupling of complex fluid flow with chemistry poses a severe challenge to turbulent combustion research. Hundreds of chemical species may react simultaneously on spatial and temporal scales spanning several orders of magnitude. For the modeller this is associated with enormous computational costs and in practice one relies on approximations and simplifying model assumptions [1]. For low Reynolds number flows it has recently become possible to solve the Navier Stokes equations directly in so called Direct Numerical Simulations (DNS) on supercomputers. Complex chemistry may be treated in DNS but this restricts calculations to two dimensions and simple geometries. In Reynolds averaged approaches (RANS), the Navier-Stokes and species conservation equations are averaged to obtain mean quantities of interest. This is a tremendous challenge because of the high non-linearity of the chemical reaction terms and the closure problem, which is introduced because averaging over correlated quantities, which are fluctuating due to turbulence, introduces new unknowns. This is one of the major reasons why simultaneous measurements on several scalars is useful in turbulent combustion research since conditional averages may be performed and correlations can be studied experimentally (see also Chapter 14). Another promising theoretical approach are so called Large Eddy Simulations (LES). LES can be viewed as a mixture of DNS and RANS: Here the computational resolution is lowered to match only sizes of large energetic eddies in the flow, which are treated as in DNS. Smaller structures, which are not resolved on the computational grid – an example may be the flame's

thin reaction zone, where the heat release takes place – require modelling assumptions (so called subgrid scale models) similar to RANS.

Much of the physical input into this research and in the construction of models has come from the application of planar laser imaging techniques. Be it interactions of flame fronts with vortices, the identification of important reactions responsible for heat release, the diffusion of species to and from the flamefront, etc., in most of the research on these topics planar imaging techniques have played an important role.

The principle of planar imaging is to form a thin sheet of light, which intersects the flame of interest and is incoherently scattered by particulates in the flame (atoms, molecules, native or seeded species). This scattered light is registered on a two-dimensional array detector and can yield information on species concentrations, temperature, and flow velocities. Most incoherent measurement techniques have been applied in this fashion, examples are Raman, Rayleigh, laser-induced fluorescence (LIF), laser-induced incandescence (LII), and Mie scattering. The present chapter is not intended as a review of these techniques but focuses on their development and application to yield multi-dimensional information on scalars in space and in time. The ability to measure several scalars at once, to resolve measurements in three dimensions, and to make time-correlated measurements allows new aspects of combustion theory to be probed and indeed may help the development of novel, more accurate models. Experimentally turbulent combustion is just as challenging as it is for the theorist: Spatial and temporal resolution requirements, the need for multiple excitation and detection systems, and the complex procedures for the extraction of quantitative data are reasons why the number of multiscalar, multidimensional measurements have been few in the past.

The chapter begins by providing a brief general background to the techniques to be discussed and references to relevant literature. Instrumentation specific for multidimensional measurements is then discussed. Examples are presented covering multi-species 2D-Raman measurements, combined particle imaging velocimetry (PIV) and planar LIF (PLIF) measurements, time resolved measurements of scalar concentration fields, 3D imaging techniques, and the imaging of reaction rates. An outlook is given and a discussion, on how this information is used in combination with state of the art numerical modelling.

8.2 Fundamentals

8.2.1 Theory

All techniques described in this chapter are based on two-dimensional imaging techniques, which can be realised with all incoherent scattering processes (Raman, Rayleigh, LIF, Mie, LII, etc). None of the processes will be reviewed here in any detail, rather the reader is referred to the excellent existing literature on the topic [2,3].

Briefly the signal power from any incoherent scattering process can be described as:

$$S = P_i N \eta q \sigma l \Omega,$$

where P_i is the laser power (assumed to be below saturation levels) [2]. N is the number density of the scattering species giving rise to the signal S. Usually N is temperature (T) and pressure (p) dependent and thus temperature, density and concentration information may be recovered from the signal. σ is the scattering cross section and depends on the physics of the interaction between the incident light and the medium for the process under question. In nonlinear interactions (e.g. two-photon absorption processes) it may itself depend on P_i. It

governs the signal strength and can differ by many orders of magnitude for the different processes [2]. For example a LIF process in a typical flame may be a factor 10^{15} more efficient than Raman scattering. On the other hand, a Mie-scattering experiment in the same flame may be a factor 10^6 more efficient than LIF. q in equation one is understood to include possible loss terms due to competing processes (for example, quenching collisions in LIF) and lineshape information, which depend on p, T, the presence of other species, and the wavelength of the exciting laser beam. Ω is the acceptance solid angle of the optics and l is the sampling extent, which relates to the spatial resolution. η describes the efficiency of the detection system. It depends on the detecting optics, detector quantum efficiency, electronic signal conversion efficiency, the band-pass function of the optical components used, and the lineshapes of both signal and exciting laser. Usually a calibration measurement is required to determine η.

Although the physics involved may be very complicated the processes are well enough understood for quantitative information on many important flame parameters to be extracted. Quantitative multi-scalar measurements in a point or along a line will be discussed in detail in Chapter 14 of this book. Since we are concerned with planar imaging approaches here, a few more specific comments relating to imaging are appropriate.

8.2.2 Planar imaging - practical considerations

In planar techniques it is crucial to illuminate the interaction region as evenly as possible which is tantamount to keeping P_i in equation 1 as constant as possible throughout the measurement plane. Several techniques have been employed to achieve this. In Raman and Rayleigh scattering, multiple beam pass configurations may be employed [4]. An advantage is that very large spectral power densities may be obtained whilst laser beam inhomogeneities are effectively averaged out. In clean, non-sooting flames this scheme can

be very effective. However, alignment is difficult, and, if present, the beam suffers cumulative absorption in the medium. Furthermore, density - and thus refractive index - gradients can lead to beam walk and degraded spatial resolution. Another technique, which shares some of the advantages of the multi-pass cell, is to form the laser illumination sheet inside the laser cavity [5]. This scheme has been applied using a flashlamp-pumped dye laser and gives sheet uniformity similar to that obtained with a multipass cell while being easier to align. When compared to a typical laser configuration with the sheet-forming optics outside the cavity, the beam waist was shown to be comparable, while the intensity was increased by more than a factor of five.

In some instances a laser beam has been swept mechanically by means of a moving mirror or electro-optically throughout the measurement plane. These approaches are very limited in the present context because usually only continuous wave lasers can be employed, and the low available powers plus mechanical limitations require acquisition times which do not allow measurements in turbulent flows (see however section 8.2.4 below, where 3D imaging approaches are discussed). The most common approach is to form a 2D light sheet using a cylindrical lens telescope (see Fig. 1). This drastically reduces the available intensity and exacerbates beam profile inhomogeneities. In principle these could be removed by spatially filtering the beam but usually this is associated with unacceptable intensity losses. In practice, therefore, one relies on on-line beam profile reference measurements, which are used to normalise acquired images on a shot by shot basis. This complicates experimental set-ups and data analysis considerably, especially if multiple lasers / detectors are used.

The spatial resolution achievable depends on pixel size of the detector array, the depth of field of the collection optics, the image magnification factor, and the size of the beam waist in the interaction region. In addition, there are the potential detrimental effects of misalignment, image intensifiers, filters, and lens aberrations and distortions. Often the

spatial resolution will be degraded farther from the optic axis. For multi-camera experiments, with different optical trains, there is the additional issue of how well images correlate on a pixel-by-pixel basis. These effects vary from experiment to experiment but in general a voxel resolution of less than $(100\ \mu m)^3$ is rarely achieved. This is important to keep in mind since, for example, the thickness of a flame front or the smallest turbulence length scales, may not be resolved by this resolution. If large gradients are present below this scale, the results have to be interpreted with caution.

8.2.3 Set-up for multidimensional imaging

Figure 1 shows the principal components of a multiple scalar measurement employing two laser and detector systems (see Chapters 2, 6, 7, 15, 16 and 17 for more information on individual laser sheet imaging techniques employed here). Specifically, it shows the set-up for simultaneous particle imaging velocimetry (see Chapter 7) and high speed PLIF imaging of OH, which is the subject of section 8.3.5.3. An experiment designed to measure two scalar quantities simultaneously would look similar in principle, with wavelengths and detectors adapted accordingly.

Focusing on the PLIF part for a moment, one sees that the frequency doubled output from a Nd:YAG pumped dye laser is formed into a thin light sheet traversing the flame (from left to right). OH fluorescence is captured by the top camera using an appropriate filter to cut out flame emission and laser scatter. Frequency conversion leads to beam profile degradations which, especially in the case of multiple pulse imaging (see section 8.3.5), may fluctuate from shot to shot. Beam profile referencing is then essential and Fig. 1 shows how this may be accomplished: Part of the laser energy is split off and passed through a cell containing a highly diluted dye solution. A coated beam splitter is then used in the detection path to combine the OH and dye fluorescence and the splitter is aligned to send the two

signals onto two separate regions of the same camera chip. Note that the beam and signal paths must be carefully matched to ensure a one to one correspondence between the two signals. In a post-processing step the two signals are carefully transformed and aligned on top of each other before the PLIF signal can be divided by the laser intensity profile. Other profiling techniques have been reported [6] and although complex, shot-to-shot beam profile referencing is often required to provide quantitative data.

Coming from the right the PIV laser sheets are aligned to coincide as nearly as possible with the PLIF laser. Corresponding signals (a double exposure of Mie scattering signals from particulates seeded to the flow, from which a velocity map can be constructed - see Chapter 7) are captured by the lower camera. Note that care must be taken with the overlap of the PIV and PLIF laser sheets, especially when significantly different wavelengths are used. For different wavelengths and/or different laser divergence characteristics, the beam waist and depth of focus can be significantly different for focusing lenses of similar focal length. In practice, it is often possible to obtain perfect overlap over only a portion of the illuminated sheet.

8.2.4 Three-dimensional imaging strategies

To fully resolve turbulent structures and their influence on flame chemistry, scalar measurements in three dimensions are highly desirable. Figure 2 shows a schematic set-up for achieving this. Here the laser sheet is swept through the measurement volume by means of a rapidly rotating mirror. By taking sequential exposures the PLIF signals emanating from 'slices' at different depths of the flame are recorded and a three-dimensional map of the scalar can be reconstructed. Care has to be taken to ensure that the laser sheet is swept fast enough on flow time scales and that the spacing between individual slices is smaller than half of the smallest spatial scale one wishes to preserve (Nyquist theorem). Very fast sweep rates can be

achieved using electro-optic or acousto-optic modulators, although maximal deflections are small and the devices are quite lossy. Wherever possible, cw lasers are preferable in this application simplifying synchronisation and yielding better beam profiles. However, except for Mie scattering, powers from available cw lasers are too low and in practice one nearly always has to revert to pulsed laser sources.

8.2.5 Excitation sources

Several high repetition rate laser systems are available to the experimentalist today. Commonly used devices are Nd:YAG lasers which are Q-switched twice during the flashlamp pump pulse (subsequently referred to as "double pulse option," DPO). They are particularly useful for particle tracking techniques (e.g. PIV, see Chapter 7). Time separations vary typically between 20 and 150 μs, determined by pump flash duration and gain build-up times. Pulse energies of 300 mJ are routinely possible. A variant of this scheme has recently been implemented by multiply Q-switching a ruby laser [7]. A 500 kHz series of up to 25 pulses of 25 mJ could be extracted during the flashlamp pump pulse. A related concept builds on pulse slicing the cw- output of a Nd:YAG laser and injection seeding the output into flash lamp pumped amplifier units [8]. Bursts of up to thirty 1 mJ pulses at 1 MHz repetition rate could be produced in this way. For high speed time correlated point measurements of scalar concentrations a 100 MHz modelocked Ti:sapphire system has been described [9]. High repetition rate excimer lasers are promising tools, operating at up to 5 kHz with a few mJ per pulse. However these repetition rates limit applications to relatively low Reynolds number flows. Cu vapour lasers have repetition rates of around 50 kHz and excellent beam properties but energies are limited to a few mJ per pulse at most. However, for scattering from liquid phases (e.g. in spray combustion) or high speed Schlieren and Mie scattering this is an ideal source [10]. Continuous wave lasers, such as Argon ion lasers, may

be used in strong signal applications (Mie). In a similar fashion long pulse flashlamp pumped dye lasers have been used for 3D imaging experiments, by exposing the detector several times during the pulse duration [11]. These lasers can produce relatively energetic pulses (1-10 J) with a duration of several microseconds. This pulse duration is short enough to resolve most flow time scales and yet long enough take advantage of the rotating mirror/fast detector approach shown in Fig. 2. A disadvantage of these systems, however, is the change in sheet intensity over the pulse (and thus the sheet location), and the difficulty of obtaining wavelengths in the ultraviolet spectral region.

A flexible system to provide pulse bursts at arbitrary time separations is to use a cluster of several Nd:YAG lasers whose output beams are combined into a single beam [12]. Results presented here were obtained with a system of four double pulsed Nd:YAG units. A patented beam combining scheme [13] results in minimal energy loss since fundamental (1064 nm) and second harmonics (532 nm) are overlapped sequentially by dichroic mirrors. The high output power system is scalable and can be synchronised to almost any external events. The outputs at 532 nm can be used directly, or, optionally can be doubled to 266 nm. Temporal separations of pulses from the 4 cavities can be arbitrarily chosen from 0 to 100 ms. If the DPO option is selected (giving 8 pulses in total), the limitations are as discussed above for PIV lasers (25 to 180 μs between double pulses). For a full discussion of the system see [14]. Tuneable radiation has been obtained by pumping a single dye laser system [12,14], which can optionally be frequency doubled. Although the dye laser was specifically modified for this purpose, this approach is problematic, since at pumping rates above ~10 kHz, even the fastest dye circulation systems will not achieve a complete replenishment of dye solution between pulses and 'memory' effects significantly degrade performance during a burst sequence. This is thought to be due to bleaching and refractive index changes (heating!), and not intersystem crossing effects, as observed in cw pumping [15]. Note that dye jet

techniques used in cw-applications cannot be used to overcome these problems since power densities are far too high. For high speed imaging with the present system, on line beam profile referencing as described in the previous section is absolutely essential. A multiple dye laser approach is ultimately more useful, but at higher cost, and much increased complexity.

8.2.6 Detector technology

Image intensification is essential to reach short exposure times and good light sensitivity. Intensified video cameras are available, but their maximum repetition speeds (5 kHz at useful image sizes) and low image resolution limit their use for precise measurements in turbulent combustion. Today CCD devices are almost universally used and these represent the bottleneck in high-speed imaging: A large dynamic range requires slow readout speeds for the charge stored on the CCD. One therefore always has to compromise between dynamic range and framing speed (the rate at which consecutive exposures can be taken).

Mechanical concepts have been used in the past where the image is swept across a length of film at high speed by a rotating mirror. This concept has been revived recently by replacement of film with a series of intensified CCD units (ICCDs), making the system much more light sensitive. The system is easily scalable but a disadvantage is the difficult synchronisation to arbitrary external events.

An alternative approach is to divide and spatially separate the image by means of beam splitting optics and to detect different temporal events at different spatial locations. The detectors are individually gated to record temporally separated events. Such a system was employed for the work presented here [16]. Up to 8 images can be acquired at arbitrary repetition rates up to about 100 MHz with this system. An optional, sequentially gated image

intensifier at the input increases the cameras sensitivity to the single photon level, but reduces detection speeds to 1 MHz, and the dynamic range to about 8 bits. This approach is difficult to scale and the signal available to each channel is reduced by a factor corresponding to the number of image divisions. But on the other hand it offers complete flexibility in terms of synchronisation to arbitrary external events and each ICCD may essentially be operated independently of the others.

A different approach is so called frame transfer technology. Here, a light sensitive pixel is surrounded by 'memory pixels' to which the recorded charge can quickly be transferred. Frame transfer chips with up to 32 memory locations have been created [17] with maximum framing rates of 1 MHz. A problem is the severe loss of photo-active area on these devices, which limits resolution and sensitivity. However, with continuing advances in VLSI (very large scale integration) and microlens-array fabrication this technology may well become the most widely used approach in the future.

For all of these detection systems, the theoretical limit on sensitivity of the measurement is related to the photon shot noise statistics of the signal. Highly sensitive detectors are particularly important for scattering mechanisms with small cross sections (such as Raman scattering) or in cases where trace species are being measured. Many of today's detectors approach these limits quite closely. In particular CCD detectors are available with quantum efficiencies of 50-90% and sixteen-bit dynamic range (>64,000). In many combustion experiments, however, the high quantum efficiency available on CCDs cannot be fully utilized because the need for high-speed gating necessitates the use of an image intensifier. While image intensifiers can be gated on nanosecond time scales (which is good for rejecting stray light from luminous flames) their quantum efficiency tends to be in the range 20-40% depending on wavelength. In addition, image intensifiers tend to degrade both the dynamic range and spatial resolution of the detection system significantly. CCD detectors

with inter-line transfer capabilities can be used to provide electronic gating of the detector directly, but currently do not have high enough stray-signal rejection capabilities for some applications. In an effort to address some of the problems inherent with intensified imaging systems, recent progress has been made with high-speed mechanical shutters, particularly for use in line-imaging applications [18].

8.3 Applications

8.3.1 Major species

Although spontaneous Raman scattering is an extremely week process, it has the advantage that the signals are readily interpreted (i.e., they are not affected by quenching processes). In principle, all major species can be monitored using a single laser wavelength. With the simultaneous detection of the much stronger Rayleigh signal, temperature can also be inferred [19]. In practice, Raman signals are so weak that even with the most energetic lasers coupled with intracavity or multipass cell configurations, two-dimensional imaging of only one or two major species has been possible to date. The largest available Raman signal in flames is often from the fuel, due to its relatively high concentration and favorable cross-section. A number of flame structure studies using fuel Raman scattering combined with simultaneous minor species measurements have been done by Schefer and co-workers [20,21].

8.3.2 Mixture fraction / temperature

One parameter of significant importance in modeling turbulent nonpremixed flames is the mixture fraction, ξ, defined as the mass fraction of all atoms originating from the fuel stream. The mixture fraction has been determined at a single point from measurements of the major species using spontaneous Raman scattering [22,23]. The single-point statistics from these studies are

among the most complete sets of experimental data available in turbulent nonpremixed flames and are used widely to verify and refine computational models. The data from single-point measurements are incomplete, however, because of the lack of multi-dimensional information required to obtain gradients. The scalar dissipation, χ (defined as $\chi = 2 D \nabla Z \cdot \nabla Z$, with D the diffusivity), determines the rate of molecular mixing and is important in modeling turbulent reacting flows. Therefore, techniques capable of two-dimensional or preferably three-dimensional measurements of the mixture fraction are needed.

Stårner *et al*. [24] demonstrated that, in some cases, the mixture fraction and temperature can be determined from simultaneous measurement of only two quantities. The method assumes unity Lewis number and a one-step reaction between fuel and oxidizer. The two measured quantities are used to form a conserved scalar from which the mixture fraction and temperature are determined in an iterative process. The scalars most widely used are the fuel concentration and Rayleigh scattering, which can be imaged simultaneously using the multi-parameter imaging configurations discussed earlier. The fuel concentration has been obtained using laser-induced fluorescence of the fuel or a fuel marker, or Raman scattering from the fuel. The fuel fluorescence approach (e.g., from acetone or acetaldehyde) provides high signal levels and has proven useful for overall fuel visualisation studies [25]. For mixture fraction determination, however, this technique is plagued by reaction and pyrolysis of the fluorescing species rich of the stoichiometric contour. The use of Raman scattering to determine the fuel concentration allows the use of simpler fuels, resulting in less severe pyrolysis problems [26].

Accurate determination of scalar gradients requires images with high signal/noise. Because of the inherent weakness of the Raman signal, there is a need to maximize the laser sheet intensity, light collection efficiency, as well as the image processing. These experiments are a good candidate for the intracavity laser configuration described above. In order to further increase

the signal/noise ratio in the Raman data, some degree of smoothing is desirable. Because the Raman and Rayleigh images are highly correlated in the regions where the Raman signal is non-zero, the Rayleigh image can be used to optimize the smoothing of the Raman image. By performing smoothing of the Raman image along constant intensity contours derived from the Rayleigh image, it has been shown that it is possible to increase the signal/noise by a factor of 10, while retaining the gradient information [27].

The two-scalar approach has been used to measure scalar gradients in a number of different flame configurations, including lifted methane diffusion flames [28], hydrogen diffusion flames [29], and piloted nonpremixed methane-air flames [30]. For this last flame, a sample of the temperature, mixture fraction, and scalar dissipation are shown in Fig. 3. To gain further insight into the mixture fraction results, other scalars have been measured simultaneously by the addition of additional cameras and laser sheets [31,32].

8.3.3 Minor species

Measurement of minor species using planar laser-induced fluorescence (PLIF) has been one of the most active and productive areas of laser diagnostics since the first demonstrations of planar OH fluorescence were reported in the early 1980s [33, 34, 35]. For a review of measurable species using LIF, refer to Chapter 2; overviews on PLIF can be found in [36, 37, 38]. In general, quantitative fluorescence measurements must take the effects of nonradiative quenching into account. For some species, however, judicious choice of the particular fluorescence transition pumped can minimise quenching effects to a level where the species concentration can be considered to be directly proportional to the fluorescence intensity (to within acceptable error bounds) [39,40]. Choice of the proper transition is important, and requires detailed knowledge of the quenching behavior as a function of temperature, pressure, and local species environment.

Fortunately, significant work has been done in this area, and 'user-friendly' quenching models are available for a variety of important combustion species [41].

Because of the complexity of turbulent flames, the measurement of a single species can often lead to ambiguities in interpretation. Therefore, in the past several years there has been an increased emphasis on combining several simultaneous planar imaging techniques to provide data that are interpreted more readily and completely. As an example of this work, Donbar *et al*. [42] combined CH and OH imaging in a turbulent nonpremixed jet flame. The boundary between the two species was used to reveal the location of the stoichiometric contour as shown in Fig. 4. In addition to simultaneous mapping of combustion intermediates such as OH and CH, several groups have done studies involving simultaneous imaging of minor species (with PLIF) and temperature (via Rayleigh scattering). This is applicable to both premixed [43] and nonpremixed [44] flames. Böckle *et al.* [45] have taken this a step further, with simultaneous measurements of OH, NO, and temperature in a swirling natural gas flame.

8.3.4 Reaction rate imaging

A topic of fundamental interest in flame research is the localisation of particular reactions taking place in a flame and also the rates at which these reactions occur. For this purpose it does not suffice to measure the concentration field of a single reactive intermediate alone as nothing is usually known about the time history between the instant the species was formed and the measurement instance. It has become possible to directly localise forward reaction rates R_f of the form:

$$R_f = n_A n_B k_f(T)$$

where n_A and n_B are the concentrations of the reactants A and B forming products and $k_f(T)$ is the (temperature dependent) forward reaction rate constant. The principle of reaction rate

imaging is as follows: The concentration fields of A and B are measured yielding fluorescence intensities S_A and S_B respectively. One has to use transitions such that the product $S_A \cdot S_B$ mimics R_f – in this case the product image intensity is proporational to the forward reaction rate. The technique has been demonstrated to image the reaction CH_2O + OH in a flame [46] which was found to correlate very well with the amount and location of the flame heat release. The technique has been extended to measure the rate of the primary CO_2 forming reaction in methane air flames, namely CO+OH $\rightarrow$ CO_2+H [47].

An example of this approach is shown in Fig. 5. It shows simultaneous single-shot two-photon CO PLIF and OH PLIF images obtained in a laminar premixed methane/air V-flame (Φ=1.45) with 10% nitrogen dilution by volume. The flame is perturbed by a counter-rotating line vortex pair propagating from the lower right towards the upper left of the images. The pixel-by-pixel product of the OH and CO PLIF images yields an instantaneous 2D measurement of the forward reaction rate R_f. The results reveal that unburned mixture remains in the core of each vortex and is subsequently consumed. Most of the trailing channel of unburned mixture, which was formed as the vortex pair entered the V-flame, has been consumed and only a small indent in the V-flame remains. The reaction zone is concentrated in regions surrounding each vortex core and extends towards the location where the vortex entered the V-flame.

8.3.5 Time domain imaging

Very few experiments have been performed so far in the time domain in turbulent combustion research. Partly this is due to the high complexity and cost of such research, but also because classical RANS modelling approaches employ temporally uncorrelated quantities, such as mean and variance, for the construction of so called probability density functions (PDF's). However, the closure model assumptions employed in RANS are far from

being satisfactory yet and it is precisely the correlations of turbulently fluctuating quantities that give rise to problems. Such correlations can only be resolved with time resolved measurements. Furthermore, since DNS and LES approaches also yield information in the time domain, such data is ideally suited for comparisons with these approaches. Finally, time resolved imaging provides insight into fundamental processes and may also be used in a practical sense: The combustion engineer may use it to monitor design faults, or in engine research to monitor variations and instabilities within single combustion cycles, to name but two examples.

Point measurements of time correlated quantities in turbulent flames have been reported [9] using an 80 MHz repetition rate Ti:Sapphire laser system. The technique, termed picosecond time-resolved LIF (PITLIF – see Chapter 5) allows detailed time correlations of scalars to be established and measurements on turbulent fluctuations. Few experiments have been performed in the past, which allow temporal *and* spatial correlations to be established in one measurement. Along a line, double pulse line images of majority species and temperature in turbulent jet flames have been recorded by Brockhinke *et al.* [48].

2D double pulse imaging techniques have also been employed, for example to measure the temporal development of OH concentration fields, from which turbulent fluctuation time scales could be measured [49, 50]. The latter OH technique has been used in combination with double pulse acetone PLIF to follow the dynamics of *un*reacted mixture as well [51]. Similarly, experiments combining Raman of CH_4 and PLIF imaging of CH to follow the evolution of large scale vortical structures in turbulent CH_4 / air flames have been reported [52]. Two-pulse temperature imaging using Rayleigh scattering has been reported by Komiyama *et al*. [53].

Periodically forced flows can be imaged sequentially using single laser and detection systems, which are phase locked to the periodic force field. Such experiments have provided valuable information on the response of the flame front to vortex perturbations or the effects of stretch and strain rates on reaction rates [54, 55]. Phase-locked detection has furthermore been used to assess resonant interactions on turbulent combustion in lean premixed combustion [56, 57].

There are very few examples of longer sequence recordings of true turbulent reactive flow structures. 2D time series measurements of fuel concentration have been reported by Winter and Long using Mie scattering of aerosols seeded into the fuel [58]. Similarly OH and O_2 were imaged at low repetition frequencies (250 Hz) by Kychakoff *et al.* [59]. Using the experimental concepts described in sections 8.2.3-8.2.6 high quality PLIF image sequences of flame produced radicals can nowadays be recorded at repetition rates exceeding 10's of kHz [12]. The following sections review some example measurements performed with this approach.

8.3.5.1 Study of flame stabilisation dynamics

The stabilisation of lifted turbulent diffusion flames is a topic of great practical and theoretical interest. Although several mechanisms have been suggested [60] the process is still far from being understood. It may be a consequence of several processes, including flamefront-vortex interactions, entrainment of fuel or combustion products, and the competition between reaction and mixing time scales. Despite much progress in recent years, these mechanisms are far from being understood. In this section we show how time resolved planar imaging techniques are capable of providing unique insight into these processes.

In Fig. 6, three series of OH radical concentration fields from a lifted H_2/air turbulent jet flame are shown, using the PLIF imaging system described in [12]. The images capture one

side of the flame, near the lift-off region (y/d~6.5). Taking the center of the conical nozzle (d = 2 mm) as the geometrical origin in the exit plane, each image corresponds to a region stretching from x = -13 mm to 1.2 mm and y = 14 mm to 27 mm at an image size of 576 times 384 pixels. Flow rates were 125 slm (standard liters per minute) of pure H_2 into air (Re=13,500 in the exit plane). The spatial resolution on the imaged region is approximately 60 μm (achieved by careful focusing and spatial filtering of the beam profile used in the experiment). It is interesting to compare this value to estimated Kolmogorov scales η for this flame situation which vary from 30 to 120 μm over the imaged x-scale at lift off height (increasing from the center of the jet outwards). Note that this implies that the technique has the required resolution to measure true scalar dissipation rates χ ('true' in 2 dimensions!) if mixture fraction were imaged, especially if one uses the often made assumption that a resolution of ~10 η suffices for this purpose [61].

The movie-like sequences shown in Fig. 6, imaged at 30 μs intervals, reveal several processes, taking place in the jet flame. In the first series one can clearly follow the formation and propagation of a thin "leader" which is propagating upstream (whilst the main combustion products are convecting downstream) and curved towards the fuel stream (images f, g, h). The propagation takes place along a contour of lean mixture but is eventually stopped by a vortex, which is forcing the flame to curve inward towards the fuel stream. This process was observed on numerous recorded sequences. It ensures that hot combustion products are fed towards the center of the flow, which can subsequently be ignited. In the second sequence, the combustion of mixed gases entrained in a large vortical structure can be seen, which may have been ignited by this process. Finally, in the last sequence very fast processes of extinction and re-ignition can be observed which demonstrate the capabilities of the technique. Large strain rates and movement of vortices lead to continuous disruptions of the flame front whilst turbulent mixing of hot products with

unburnt mixture can lead to re-ignition. Note that out of plane motion cannot be captured with two-dimensional imaging techniques, and three-dimensional information would offer a more complete picture on the flame dynamics (see section 8.3.6).

8.3.5.2 Ignition phenomena

Figure 7 shows an application of the technique to study ignition phenomena in turbulent mixtures of methane and air and comparisons to DNS calculations under similar conditions [62]. Stoichiometric mixtures of CH_4 and air were ignited in a large combustion vessel fitted with 4 high speed fans to impart controlled amounts of turbulence on the mixture. Sequence a) shows the evolution of the OH concentration field captured by high speed PLIF imaging. The colour coding refers to the OH mole fraction and was obtained by calibration against measurements from laminar flame kernels [63]. Note the very high concentration of OH initially because of the intense heat of the spark during ignition, which decreases to equilibrium values as the flame is established. The initially laminar flame kernel becomes more and more wrinkled as it is propagating through the turbulence field. In b) the OH concentration field obtained by a DNS simulation for similar conditions is shown for comparison. Complex chemistry (17 species, 52 reactions) is treated in the presence of homogenous isotropic turbulence in two dimensions and a model is included for energy deposition during the spark. The computational domain was 1 cm^2. In c) the predicted CH_2O concentration field is shown for the same event, d) corresponds to the vorticity field (corresponding to u'=3 ms^{-1}). Although comparisons of individual sequences as shown can only be made in a qualitative sense, the main trends of the observed phenomena are predicted by the calculations. For example OH concentration values, and the appearance of the first negatively curved wrinkles on the flame front (corresponding roughly to one turnover time τ of the most energetic eddies in the flow) are similar in both experiment and simulation.

Using statistical analysis of such data one can, for example, quantify the progress of flame wrinkling. The latter is defined as the ratio of the flame surface area of the turbulent flame to the corresponding area of a laminar flame and can be directly obtained by integration of the flame contours using, for example, the image analysis methods presented in [64] and [65]. The degree of flame wrinkling is directly related to local reaction rates. The reaction boundary can also be used to define a reaction progress variable c which is defined as $c = 0$ for fresh gases (corresponding to regions outside the detected flame boundaries in the examples presented here) and $c = 1$ for burnt gases (inside the boundaries). The conservation equations for premixed flames may be directly expressed in terms of such a progress variable. For LES this equation may be filtered so that only large scale structures are preserved and a model assumption is used to include the effects of small scale wrinkling in the calculation (a so called subgrid scale model). Knikker *et al.* [66] have shown how experimentally determined progress variables may be used to validate such subgrid scale models.

8.3.5.3 Combined time-domain / PIV imaging

Some of the most interesting data for phenomenological studies of flame chemistry interactions stems from the simultaneous application of 2D flow visualisation and scalar measurement techniques. An example may be the simultaneous measurement of the concentration field of a combustion produced radical and the flow velocity field. One is able to obtain detailed information on perturbations of the reaction zone structure by the turbulent flow field, and, vice versa, one is also able to "watch" chemistry effects on the fluid flow. It is precisely this coupling between fluid flow and chemistry, which makes modelling of turbulent combustion so difficult.

In repeatable, periodically perturbed laminar counter-flow diffusion flames OH PLIF and PIV measurements have been applied sequentially to assess the effect of flame stretch on

local OH concentration in the validation of laminar flamelet models [54]. The experiments verified that OH concentrations are only marginally dependent on local strain rates for low Damköhler flows, because its lifetime is longer than characteristic convection times of the flame.

In turbulent combustion such phase-locked measurement approaches are not feasible (unless resonant instabilities are studied as remarked earlier) and a set-up as shown in Fig. 1 must be used to permit simultaneous recordings of the involved quantities.

An early application of simultaneous scalar /velocity field measurements combining fuel tracer PLIF of biacetyl, and PIV in a turbulent propane / air flame has been reported in [67]. The technique can be used to map instantaneous velocity fluctuation fields and reaction progress variables. Using combined OH PLIF and PIV, model assumptions concerning counter-gradient turbulent diffusion could be investigated quantitatively [68]. By the same technique the effects of compressive strain on the reaction layer thickness could be measured [69]. Generally, diffusive, broadened out OH structures were only found in regions of low compressive strain. Watson *et al.* have used PIV in combination with CH and OH PLIF to study the lift off region of turbulent methane / air diffusion flames [70, 71] and the work indicates that the flame stabilises near the point where flow velocities approach premixed laminar flame speeds.

Despite the wealth of information that these techniques provide, they are often difficult to interpret, since data is collected at random time points and temporally uncorrelated. A novel approach is to combine time sequenced PLIF data on reaction scalars with PIV [72] an example of which is shown in Fig. 8. The two sequences shown were obtained in the TECFLAM flame [73], a turbulent non-premixed $H_2/CH_4/N_2$/air flame, which serves as an international standard for model validation purposes (see also Chapter 14 of this book).

Reynolds numbers near the fuel exit plane were approximately 20,000 for the situations shown (fuel exit velocity of 55 ms^{-1}), and the observation region situated 10 and 5 nozzle diameters downstream (top and bottom sequences, respectively, nozzle diameter 8 mm). The colour mapping indicates OH fluorescence intensity (not normalised). Images were acquired at 75 μs intervals, with the PIV laser pulses interleaving the second OH image in each sequence. Both the fuel and the co-flow (air) were seeded using 1 μm TiO_2 particles, to provide velocity measurement both in reactant and in product zones. Two different types of events leading to local extinction can be followed: In the top sequence a large scale structure moves through the flame front leading to excessive mixing of cold, unreacted species, cooling the flame front which subsequently extinguishes. In the bottom sequence one can see a thin reaction zone of an already disrupted flame which is thinned by strong compressive strain until the point where heat loss from the thinned reaction zone dominates over the heat release - with extinction as a result. It is also clearly visible that broadly structured OH features appear in regions where compressive strain is very low, (the OH lifetimes are approximately 4 times larger than convective timescales for the presented situation) [see also 69].

8.3.6 Three-dimensional imaging

To measure complete 3D scalar gradients in each point of a two-dimensional plane it suffices to record two planes spaced at less than the linear dimension of the smallest scale one wishes to preserve. The principle has been demonstrated in several studies [74,75,76]. Stereoscopic PIV imaging can furthermore be used to measure three Cartesian velocity components. As described in section 8.3.5, time domain imaging techniques can quite readily be transformed into true three-dimensional measurement techniques by sweeping a light sheet through the volume of interest at high speeds. Tomographic imaging approaches

have also enjoyed some success in the past [2, 3, 77] but will not be discussed in the present context.

Measurements based on this principle have been demonstrated in reactive and non-reactive flows using particulate (Mie) scattering from aerosols [78, 11], Rayleigh scattering [79], LIF from O_2 [59], acetone [11] and biacetyl [59,78]. High resolution quantitative measurements of soot volume distribution have been conducted by Hult, *et al.* using LII [80]. An example from this approach is shown in Fig. 9. The experiment was conducted in a turbulent ethylene air diffusion flame, diluted with N_2 (64 % by volume of C_2H_4, 36 % of N_2 in the fuel stream). Exit velocities were 15 m/s, corresponding to *Re*~2200. Eight consecutive laser shots were used at 12.5 μs intervals with sweep rates adjusted to yield 0.4 mm separations between consecutive measurement planes. No significant fluid flow could take place during overall acquisition times. The LII signals were calibrated against laminar reference flames to yield absolute soot volume fractions. Since the soot is primarily formed towards the fuel rich side near the stoichiometric air/fuel boundary in a non-premixed flame, the large scale soot structures seen in the image are due to wrinkling of this boundary by the turbulent flow. The lower row in Fig. 9 shows Cartesian gradients in x, y and z as well as the reconstructed true 3D gradient obtained from these images. In Fig. 10 the reconstructed isoconcentration surfaces corresponding to 1, 2 and 3 ppm soot volume fraction are displayed, highlighting the amount of topological detail that can be obtained using the technique.

8.4 Conclusions, future outlook

Only recently have the computational tools developed to a point where a close coupling between detailed multi-dimensional experiments and computations seems feasible. Along with rapid advances in computations, diagnostic capabilities have also increased enormously

over the past decade. The availability of new laser sources, detectors, and data processing schemes allows acquisition of more accurate data, and measurements that can be more specifically tailored to the needs of the modeling community. The measurement techniques described in this chapter allow the acquisition of scalar and velocity fields in two as well as three dimensions, which may furthermore be time resolved on scales relevant for combustion situations of practical relevance.

A major motivation of this work is that it provides a more stringent and rigorous test for novel modeling approaches than has hitherto been possible. The new data generated from complex, challenging flows can be more directly compared to numerical data (as shown in the example of spark ignition in this chapter) clearly highlighting merits and failings of new theoretical approaches. A big challenge for this kind of direct comparison, however, remains in the complete specification of the boundary conditions. Unlike laminar flames or forced time-varying flames, a direct detailed comparison of multidimensional measurements and computations of fully turbulent flames remains beyond current capabilities.

However there may yet be a more important motivation for the presented work: Time resolved planar imaging or simultaneous measurements of multiple scalars in several dimensions will help to uncover yet undetected physical phenomena in turbulent combustion from which new models can be constructed. For example time sequenced imaging of combustion instabilities in rocket engines, ultra lean burning gas turbines, furnace pulsed combustors, or new ignition concepts in internal combustion engines will provide important insight into the immensely complex flows prevailing in these devices. The concept of flamelets serves as an important example on how an experimental observation (much of it based on planar imaging techniques!) has led to the construction of a highly successful theoretical modeling tool. In much the same way the new techniques may open our eyes to

new phenomena and promote new understanding, which could lead to better combustion devices.

8.5 Figures

1. Candel, S., Thévenin, D., Darabiha, N., and Veynante, D., "Progress in Numerical Combustion," *Comb. Sci. and Tech.*, vol. 149, pp. 297-337, 1999.

2. Eckbreth, A.C., "Laser Diagnostics for Combustion Temperature and Species," 2nd edition, Gordon and Breach Publishers, Amsterdam, 1996.

3. Taylor, A.M.K.P., "Instrumentation for Flows with Combustion," Academic Press, London, 1993.

4. Winter, M., Lam, J.K., and Long, M.B., "Techniques for high-speed digital imaging of gas concentrations in turbulent flows," *Exp. Fluids*, vol. 5, pp. 177-183, 1987.

5. Marran, D.F., Frank, J.H., Long, M.B., Stårner, S.H., and Bilger, R.W., "Intracavity Technique for Improved Raman/Rayleigh Imaging in Flames," *Opt. Lett.,* vol. 20, pp. 791-793, 1995.

6. Stårner, S H., Kelman, J B., Masri, A R., and Bilger, R W., "Multispecies measurements and mixture fraction imaging in turbulent diffusion flames," *Exp. Thermal & Fluid Sci*., vol. 9, pp. 119-124, 1994.

7. Huntley, J.M. “High speed laser speckle photography: Part 1: Repetitively Q-switched ruby light source,” *Opt. Eng*., vol. 33, pp. 692-1699, 1994.

8. Wu, P.P. and Miles, R.B., “High energy pulse-burst system for megahertz-rate flow visualization,” *Opt. Lett.*, 25, pp. 1639-1641, 2000.

9. Renfro, M.W., Guttenfelder, W.A., King, G.B., and Laurendeau, N.M., “Scalar Time-Series Measurements in Turbulent $CH_4/H_2/N_2$ Nonpremixed Flames: OH,” *Combust. Flame,* vol. 123, pp. 389-401, 2000.

10. Reeves, M., Towers, D.P., Tavender, B. and Buckberry, C.H., “A Technique for Routine, Cycle-Resolved 2-D Flow Measurement and Visualisation within SI Engine Cylinders in an Engine Development Environment,” Proceedings of the 10th International Symposium on Turbulence, Heat and Mass Transfer, Lisbon, 2000.

11. Patrie, B.J., Seitzman, J.M., and Hanson, R.K., “Instantaneous three-dimensional flow visualization by rapid acquisition of multiple planar flow images,” *Opt. Eng*., Vol. 33, pp. 975-980, 1994.

12. Kaminski, C.F., Hult, J., and Aldén, M. “High Repetition Rate Planar Laser Induced Fluorescence of OH in a turbulent non-premixed flame,” *Appl. Phys. B.,* vol. 68, pp. 757-760, 1999.

13. Proprietary beam combination scheme of Thomson CSF Laser systems, France.

14. Hult, J., “Development of Time Resolved Laser Imaging Techniques for the Study of Turbulent Flames.” Lund Reports on Combustion Physics, LRCP64, Lund Institute of Technology, Sweden, 2000.

15. Schäfer, F.P. (ed.), “Dye Lasers.” Topics in *Applied Physics Series*, vol. 1, Springer Verlag, Heidelberg, 1989.

16. Patent property of Hadland Photonics, U.K.

17. Gord, J.R., Tyler,C., Grinstead Jr., K.D., Fiechtner, G.J., Cochran, M.J., and Frus, J.R., “Imaging strategies for the study of gas turbine spark ignition,” SPIE paper 3783-43, 2000.

18. Miles P.C., and Barlow, R.S., “A fast mechanical shutter for spectroscopic applications,” *Meas. Sci. Technol*., vol. 11, pp. 392-397, 2000.

19. Long, M.B., Levin, P.S., and Fourguette, D.C. “Simultaneous two-dimensional mapping of species concentration and temperature in turbulent flames,” *Opt. Lett.,* vol. 10, pp. 267-269, 1985.

20. Schefer, R.W., Namazian, M., and Kelly, J., “Simultaneous Raman scattering and laser-induced fluorescence for multispecies imaging in turbulent flames,” *Opt. Lett*., vol. 16, pp. 858-860, 1991.

21. Schefer, R.W., Namazian, M., and Kelly, J., “Stabilization of lifted turbulent-jet flames,” *Comb. Flame*, vol. 99, pp. 75-86, 1994.

22. Dibble, R.W., Masri, A.R., and Bilger, R.W., "The spontraneous Raman scattering technique applied to nonpremixed flames of methane," *Comb. Flame*, vol. 67, pp. 189-206, 1987.

23. Masri, A. R., Dibble, R. W., and Barlow, R. S., "The structure of turbulent nonpremixed flames revealed by Raman-Rayleigh-LIF measurements," *Prog. Energy Combust. Sci*. vol. 22, pp. 307–362 1996.

24. Stårner, S.H., Bilger, R.W., Dibble, R.W., and Barlow, R.S., "Measurements of conserved scalars in turbulent diffusion flames," *Combust. Sci. Technol*., vol. 86, pp. 223-236, 1992.

25. Tait, N.P., and Greenhalgh, D.A., "2D Laser induced fluorescence imaging of parent fuel fraction in nonpremixed combustion," *Proc. Comb. Inst*., vol. 24, pp. 1621-1628, 1992.

26. Frank, J.H., Lyons, K.M., Marran, D.F., Long, M.B., Stårner, S.H., and Bilger, R.W. "Mixture Fraction Imaging in Turbulent Nonpremixed Hydrocarbon Flames," *Proc. Comb. Inst*., vol. 25, pp. 1159-1166, 1994.

27. Stårner, S.H., Bilger, R.W., and Long, M.B. "A Method for Contour-Aligned Smoothing of Joint 2D Scalar Images in Turbulent Flames," *Combust. Sci. Tech.,* vol. 107, pp. 195-203, 1995.

28. Stårner, S.H., Bilger, R.W., Frank, J.H., Marran, D.F., and Long, M.B, "Mixture Fraction Imaging in a Lifted Methane Jet Flame," *Combust. Flame,* vol. 107, pp. 307-313, 1996.

29. Stårner, S.H., Bilger, R.W., Long, M.B., Frank, J.H., and Marran, D.F., "Scalar Dissipation Measurements in Turbulent Jet Diffusion Flames of Air Diluted Methane and Hydrogen," *Combust. Sci. Tech.,* vol. 129, pp. 141-163, 1997.

30. Kelman, J.B., Masri, A.R., Stårner, S.H., and Bilger, R.W., "Wide-field conserved scalar imaging in turbulent diffusion flames by a Raman and Rayleigh Method," *Proc. Comb. Inst*., vol. 25, pp. 1141-1147, 1994.

31. Kelman, J.B., and Masri, A.R., "Quantitative technique for imaging mixture fraction, temperature, and the hydroxyl radical in turbulent diffusion flames," *Appl.Opt.,* vol. 36, pp. 3506-3514, 1997.

32. Fielding, J., Schaffer, A.M., and Long, M.B., "Three-Scalar Imaging in Turbulent Non-Premixed Flames of Methane," *Proc. Comb. Inst.,* vol. 27, pp. 1007-1014, 1998.

33. Aldén, M., Edner, H., Holmstedt, G., Svanberg, S., and Högberg, T., "Single-pulse laser-induced OH fluorescence in an atmospheric flame, spatially resolved with a diode array detector," *Appl. Opt.,* vol. 21, pp. 1236-1240, 1982.

34. Dyer, M.J. and Crosley, D.R., "Two-dimensional imaging of OH laser-induced fluorescence in a flame," *Opt. Lett.,* vol. 7, pp. 382-384, 1982.

35. Kychakoff, G. Howe, R.D., Hanson, R.K., and McDaniel, J.C., "Quantitative visualization of combustion species in a plane," *Appl. Opt.,* vol. 21, pp. 3225-3227, 1982.

36. Seitzman, J.M. and Hanson, R.K., "Planar Fluorescence Imaging in Gasses," in *Instrumentation for Flows with Combustion,* A.M.K.P. Taylor, ed., pp. 405-466, Academic Press, 1993.

37. Daily, J.W., "Laser induced fluorescence spectroscopy in flames," *Prog. Energy Combust. Sci*., vol. 23, pp. 133-199, 1997.

38. Wolfrum, J., "Lasers in combustion: from basic theory to practical devices," *Proc. Comb. Inst.,* vol. 27, pp. 1-41, 1998.

39. Haumann, J, Seitzman, J.M., and Hanson, R.K., "Two-photon imaging of CO in combustion flows using planar laser-induced fluorescence," *Opt. Letters.*, 11, pp. 776-778, 1986.

40 . Andresen, P., Schluter, H., Wolff, D., Voges, H., Koch, A., Hentschel, W., Oppermann, W., Rothe, E., "Identification and imaging of OH (v"=0) and O_2 (v"=6 or 7) in an automobile spark-ignition engine using a tunable KrF excimer laser ," *Appl. Opt.,* vol. 31, pp. 7684-7689, 1992.

41. Tamura, M., Berg, P. A., Harrington, J. E., Luque, J., Jeffries, J. B., Smith, G. P. and Crosley, D. R. "Collisional Quenching of CH(A), OH(A), and NO(A) in Low Pressure Hydrocarbon Flames," *Combust. Flame,* vol. 114, pp. 502-514, 1998.

42. Donbar, J.M., Driscoll, J.F., and Carter, C. D., "Reaction Zone Structure in Turbulent Nonpremixed Jet Flames - From CH-OH PLIF Images," *Combust. Flame,* vol. 122, pp. 1-19, 2000.

43. Chen, Y.-C. and Mansour, M.S. "Topology of turbulent premixed flame fronts resolved by simultaneous planar imaging of LIPF of OH radical and Rayleigh scattering," *Exp. Fluids.,* vol. 26, pp. 277-287, 1999 .

44. Namazian, M., Kelly, J., and Schefer, R., "Simultaneous NO and temperature imaging measurements in turbulent nonpremixed flames," *Proc. Comb. Inst.,* vol. 25, pp. 1149-1157, 1994.

45. Böckle, S., Kazenwadel, J., Kunzelmann, T., and Schulz, C. "Laser-diagnostic multi-species imaging in strongly swirling natural gas flames," *Appl. Phys. B.,* vol. 71, pp. 741–746, 2000.

46. Paul, P.H. and Najm, H.N., "Planar laser-induced fluorescence imaging of flame heat release rate," *Proc. Comb. Inst.,* vol. 27, pp. 43-50, 1998.

47. Rehm, J.E. and Paul, P.H., "Reaction Rate Imaging," *Proc. Comb. Inst.,* vol. 28, pp. 1775-1782, 2000.

48. Brockhinke, A., Kohse-Höinghaus, K., and Andresen, P. "Double pulse one-dimensional Raman and Rayleigh measurements for the detection of temporal and spatial structures in a turbulent H_2-air diffusion flame," *Opt. Lett.,* vol. 21, pp. 2029-2031, 1996.

49. Dyer, M.J., and Crosley, D.R., "Rapidly sequenced pair of two-dimensional images of OH laser induced-fluorescence in a flame," *Opt. Lett.,* vol. 9, pp. 217-219, 1984.

50. Atakan, B,M., Jörres, V., and Kohse-Höinghaus, K., "Double-pulse 2D LIF as a means for following flow and chemistry development in turbulent combustion," *Ber. Bunsenges. Phys. Chem.,* vol. 97, pp. 1706-1710, 1993.

51. Seitzman, J.M., Miller, M.F., Island, T.C., and Hanson, R.K., "Double-pulse imaging using simultaneous OH/acetone PLIF for studying the evolution of high-speed, reacting mixing layers," *Proc. Comb. Inst.,* vol. 25, pp. 1743-1750, 1994.

52. Schefer, R.W., Namazian, M., Filtopoulos, E.E.J., Kelly, J., "Temporal evolution of Turbulence/Chemistry interactions in lifted, turbulent-jet flames," *Proc. Comb. Inst.,* vol. 25, pp.1223-1231, 1994.

53. Komiyama, M., Miyafuji, A., and Takagi, T., "Flamelet behavior in a turbulent diffusion flame measured by Rayleigh scattering image velocimetry," *Proc. Comb. Inst.,* vol. 26, pp. 339-346, 1996.

54. Mueller, C.J., Driscoll, J.F., Sutkus, D.J., Roberts, W.L., Drake, M.C., and Smooke, M.D., "Effect of unsteady local stretch rate on OH chemistry during a flame-vortex interaction: to assess flamelet models," *Comb. Flame,* vol. 100, pp. 323-331, 1995.

55. Katta, V.R., Carter, C.D., Fiechtner, G.J., Roquemore, W.M., Gord, J.R., and Rolon, J.C., "Interaction of a vortex with a flat flame formed between opposing jets of hydrogen and air," *Proc. Comb. Symp.* 27, pp. 587-594, 1998.

56. Venkatamaran, K.K., Preston, L.H., Simons, D.W., Lee, J.G., and Santavicca, D.A., "Mechanism of combustion instability in a lean premixed dump combustor," *J. Propulsion Power*, 15, pp. 909-918, 1999.

57. Lee, S.-Y., Seo, S., Broda, J.C., Pal, S., and Santoro, R.J., "An experimental estimation of mean reaction rate and flame structure during combustion instability in a lean premixed gas turbine combustor," *Proc. Comb. Inst.*, 28, pp. 775-782, 2000.

58. Winter, M., and Long, M.B., "Two-dimensional measurements of the time development of a turbulent premixed flame," *Comb. Sci. Tech.,* vol. 66, pp. 181-188, 1989.

59. Kychakoff, G., Paul, P.H., van Cruyningen, I., and Hanson, R.K., "Movies and 3-D images of flowfields using planar laser-induced fluorescence," *Appl. Opt.,* vol. 26, pp. 2498-2500, 1987.

60. Pitts, W. M. "Assessment of theories for the behavior and blowout of lifted turbulent jet diffusion flames," *Proc. Comb. Inst.,* vol 22, pp. 809-816, 1988.

61. Tennekes, H., and Lumley, J.L., “A first course in turbulence,” MIT press, Cambridge, Massachusetts, 1994.

62. Kaminski, C.F., Hult, J., Aldén, M., Lindenmaier, S., Dreizler, A., Maas, U., and Baum, M., “Spark ignition of turbulent methane/air mixtures revealed by time-resolved planar laser-induced fluorescence and direct numerical simulations,” *Proc. Comb. Inst.,* vol. 28, pp. 399-405, 2000.

63. Dreizler, A., Lindenmaier, S., Maas, U., Hult, J., Aldén, M., Kaminski, C.F., “Characterisation of a spark ignition system by planar-laser-induced fluorescence of OH at high repetition rates and comparisons with chemical kinetic calculations,” *Appl. Phys. B.,* vol. 70, pp. 287-294, 2000.

64. Abu-Gharbieh, R., Hamarneh, G., Gustavsson, T., and Kaminski, C.F., “Flame front tracking by laser induced fluorescence spectroscopy and advanced image analysis,” *Opt. Express* 8, pp. 278-287, 2001.

65. Malm, H., Sparr, G., Hult, J., and Kaminski, C.F., “Nonlinear diffusion filtering of images obtained by planar laser-induced fluorescence spectroscopy," *J. Opt. Soc. Am. A*, vol. 17, pp. 2148-2156, 2000.

66. Knikker, R., Veynante, D., Rolon, J.C., and Meneveau, C., “Planar Laser-Induced Fluorescence in a Turbulent Premixed Flame to analyze Large Eddy Simulation Models,” Proceedings of the 10th International Symposium on Turbulence, Heat and Mass Transfer, Lisbon, 2000.

67. Frank, J.H., Lyons, K.M., and Long, M.B., "Simultaneous scalar/velocity field measurements in turbulent gas-phase flows," *Comb. Flame,* vol. 107, pp. 1-12, 1996.

68. Frank, J.H., Kalt, P.A.M., and Bilger, R.W., "Measurements of conditional velocities in turbulent premixed flames by simultaneous OH PLIF and PIV," Comb. Flame, vol. 116, pp. 220-232, 1999.

69. Rehm, J.E., and Clemens, N.T., "The relationship between vorticity / strain and reaction zone structure in turbulent non-premixed jet flames," *Proc. Comb. Inst.,* vol. 27, pp. 1113-1120, 1998.

70. Watson, K.A., Lyons, K.M., Donbar, J.M., and Carter, C.D. "Scalar and velocity field measurements in a lifted CH_4 – air diffusion flame," *Comb. Flame,* vol. 117, pp. 257-271, 1999.

71. Watson, K.A., Lyons, K.M., Donbar, J.M., and Carter, C.D., "Observations on the leading edge in lifted flame stabilization." *Comb. Flame,* vol. 119, pp. 199-202, 1999.

72. Hult, J., Josefsson, G., Aldén, M., and Kaminski, C.F., "Flame front tracking and simultaneous flow field visualization in turbulent combustion," Proceedings of the 10th International Symposium on Applications of Laser Techniques to Fluid Mechanics, Lisbon, 2000.

73. Bergmann, V., Meier, W., Wolff, D., and Stricker, W., "Application of spontaneous Raman and Rayleigh scattering and 2D LIF for the characterization of a turbulent $CH_4/H_2/N_2$ jet diffusion flame," *Appl. Phys. B.,* vol. 66, pp. 489-502, 1998.

74. Yip, B. and Long, M.B., "Instantaneous Planar Measurement of the Complete Three-Dimensional Scalar Gradient in a Turbulent Jet," *Opt. Lett.* vol. 11, pp. 64-66, 1986.

75. O'Young, F., and Bilger, R.W., "Scalar gradient and related quantities in turbulent premixed flames," *Comb. Flame,* vol. 109, pp. 682-700, 1997.

76. Su, L.K. and Clemens, N.T., "Planar measurements of the full three-dimensional scalar dissipation rate in gas-phase turbulent flows," *Exp. Fluid,* vol. 27, pp. 507-521, 1999.

77. Torniainen, E.D., Hinz, A., and Gouldin, F.C., "Tomographic analysis of unsteady reacting flows," *AIAA J.*, 36, pp. 1270-1278, 1998.

78. Yip, B., Schmitt, R.L., and Long, M.B., "Instantaneous three-dimensional concentration measurements in turbulent jets and flames." *Opt. Lett.,* vol. 13, pp.96-98, 1988.

79. Yip, B., Lam, J.K., Winter, M., and Long, M.B., "Time resolved three-dimensional concentration measurements in a gas jet," *Science,* vol. 235, pp. 1209-1211, 1987.

80. Hult, J., Axelsson, B., Omrane, A., Collin, R., Nygren, K., Bengtsson, P-E., Aldén, M., and Kaminski, C.F., "Quantitative three dimensional imaging of soot volume fraction in turbulent non-premixed flames," *Exp. in Fluids,* accepted for publication.

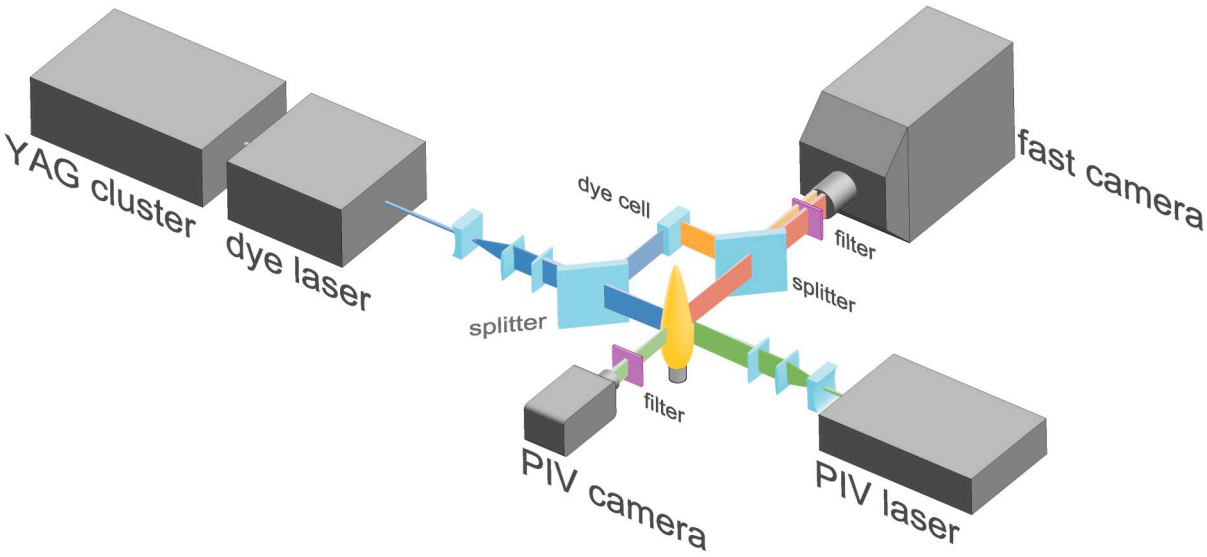

Figure 1: Multidimensional imaging set-up. The system shown allows the independent acquisition of time-sequenced PLIF imaging data and flow field data from particle imaging velocimetry.

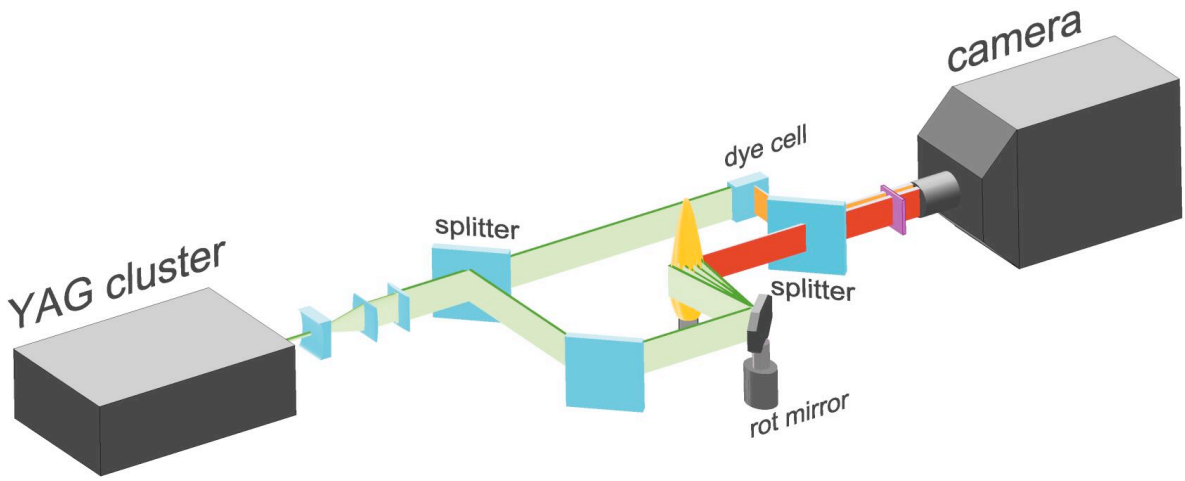

Figure 2: Schematic set-up of a 3 dimensional imaging experiment. The laser beams are spatially displaced by means of a rapidly rotating mirror.

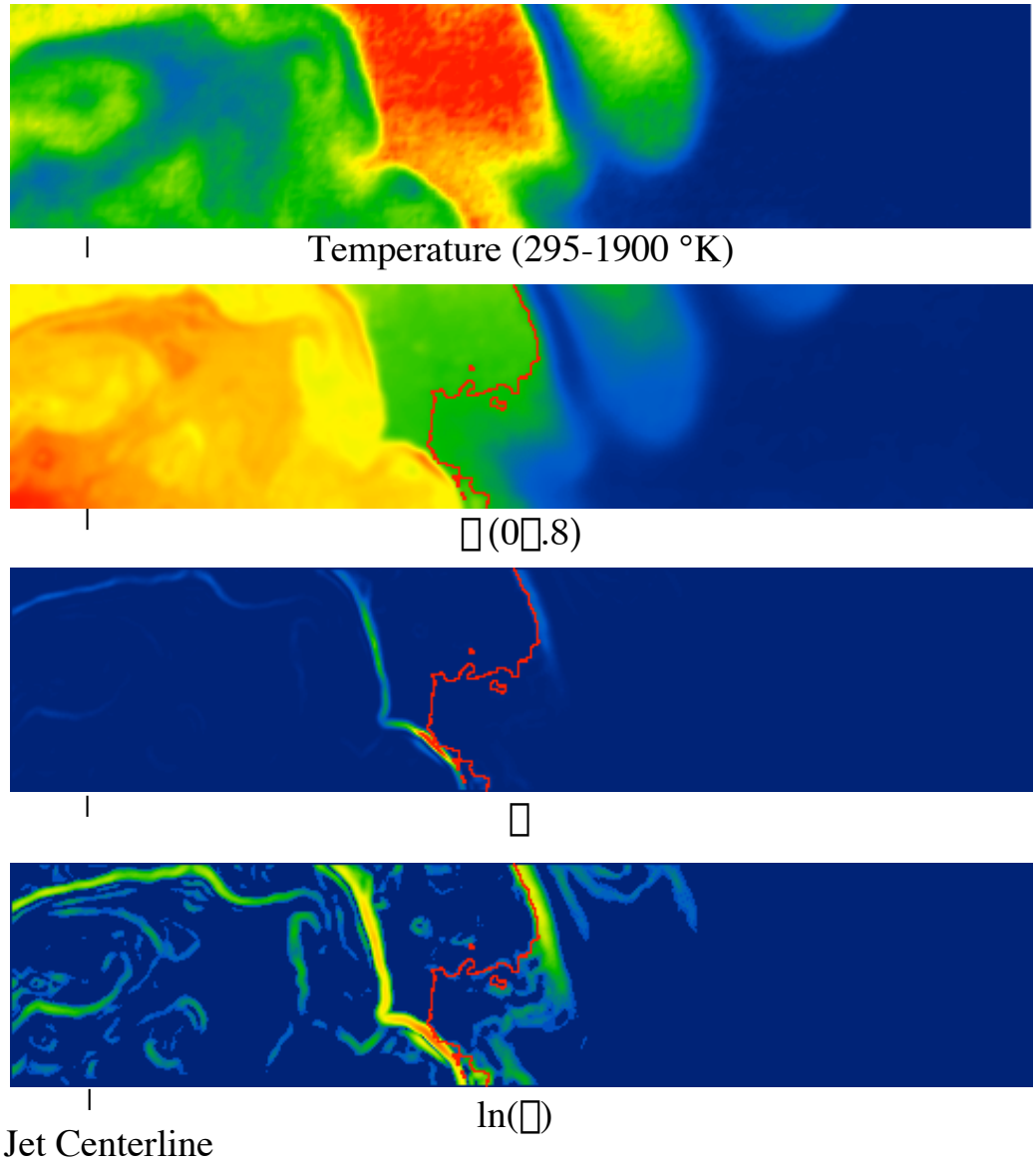

Figure 3: Images of the temperature, mixture fraction, scalar dissipation, and log of scalar dissipation. The data were obtained from simultaneous images of Rayleigh scattering and Raman scattering from methane. The stoichiometric contour is shown in red.

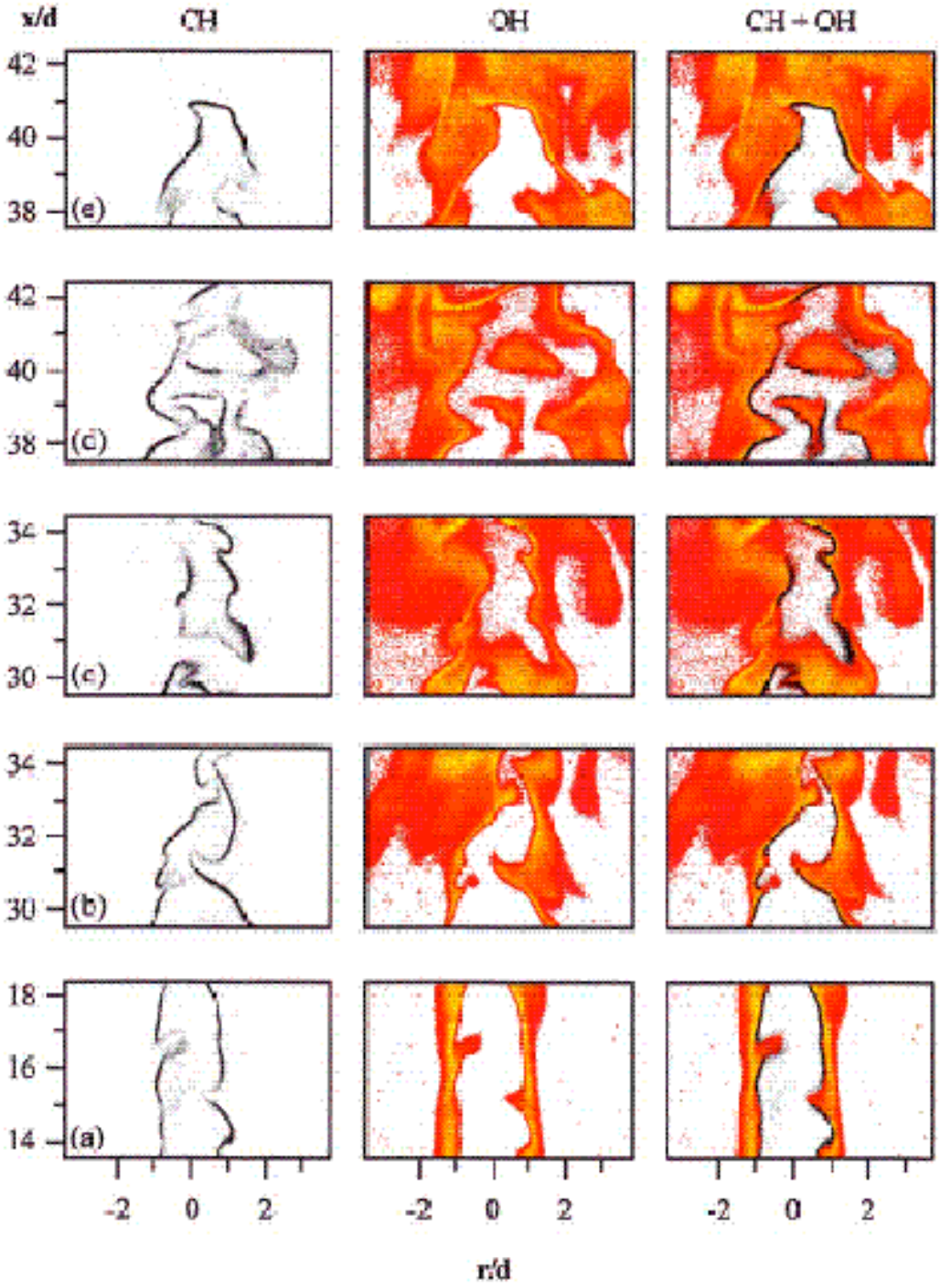

Figure 4: Structure of the simultaneous CH/OH reaction zones in the high-Reynolds-number (18,600) jet flame: left, CH; middle, OH; right, CH and OH. Each CH-OH image pair was obtained at a random time (from Donbar et. al, 2000).

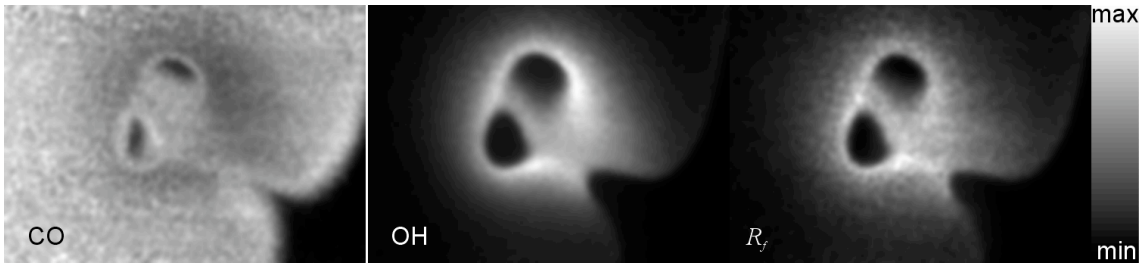

Figure 5: Example of reaction rate imaging of the CO+OH $\rightarrow$ CO_2+H reaction in a laminar premixed methane air flame, which is interacting with a pair of counterrotating line vortices. The third image above shows the product of the CO and OH PLIF images displayed to the left. The transitions were chosen such that the product image visualises the forward reaction rate (R_f). [Images are property of Jonathan H. Frank, Sandia National Laboratories, and are reproduced here with kind permission. Support for his work provided by DOE/BES Chem. Sci. Div.].

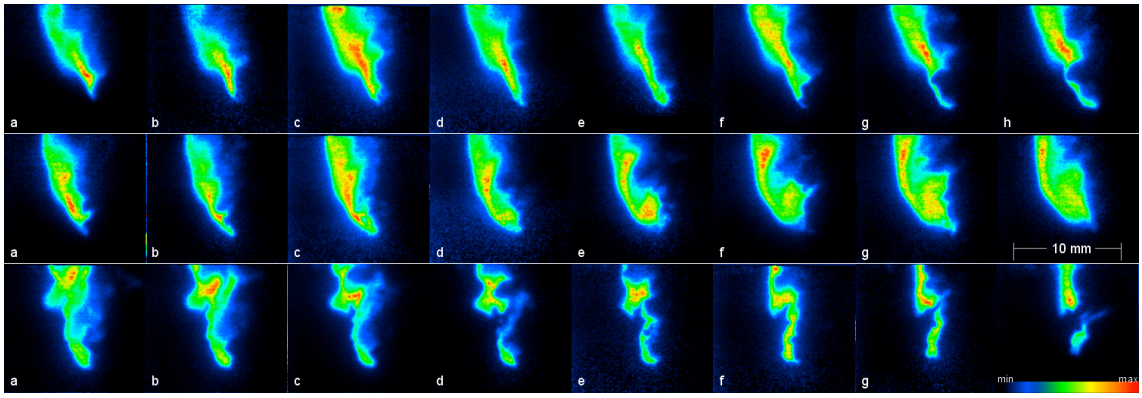

Figure 6: High speed PLIF imaging of OH radical distribution fields in a lifted H_2/air jet flame. Flow rates: 125 standard litres per minute of pure H_2 into air, corresponding to Re=13,500 (exit velocity: 670 ms^{-1}). The time difference between individual exposures is 30 μs. Shown is the OH distribution in the lift off region to one side of the burner (x= -13mm to +1.2 mm, y=14 mm to 27 mm, nozzle diameter: 2 mm)

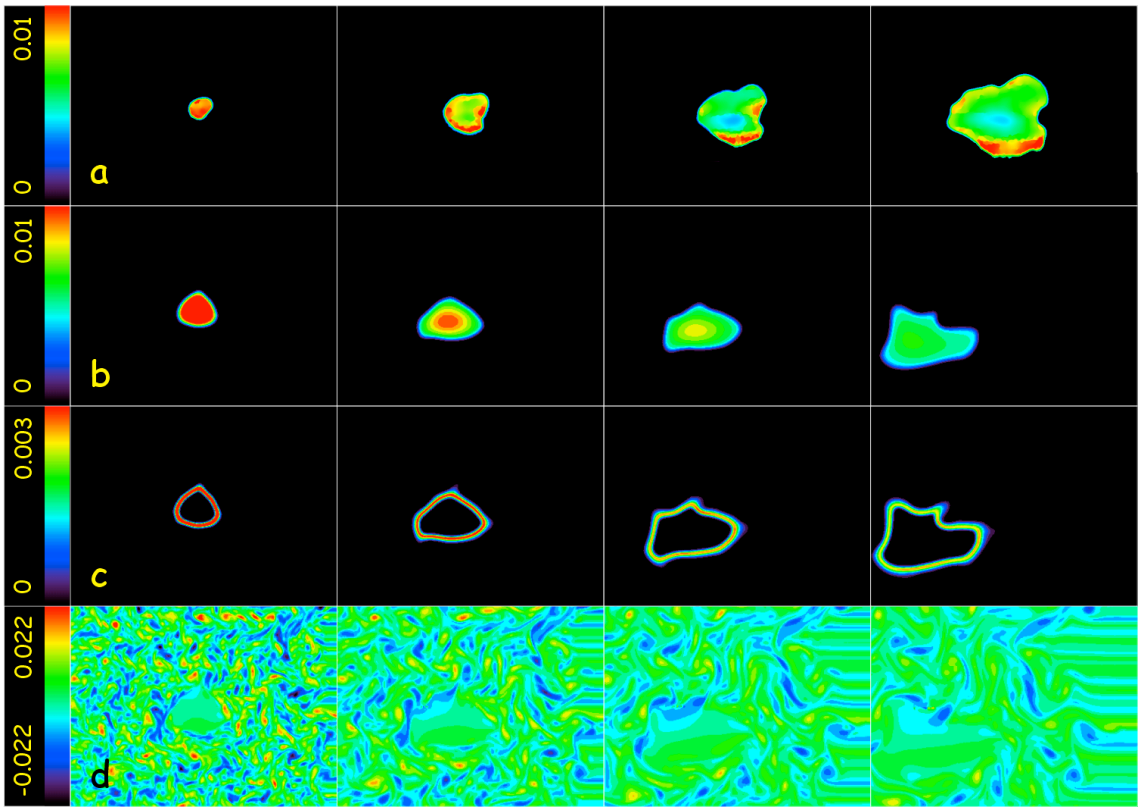

Figure 7: Comparison of a high speed PLIF sequence of the OH concentration field during turbulent spark ignition (a) and a DNS calculation under similar conditions (b-d). The shown quantities are: (a) measured OH mole fraction, (b) OH mole fraction calculated by DNS result, (c) CH_2O concentration field (DNS), (d) the calculated vorticity field (in ms^{-1}). The time scale going from left to right are t/τ=0.3, 0.6, 0.9, and 1.2, respectively, where τ is the turnover time of the most energetic eddy. The last instance in the sequences (t/τ=1.2) corresponds to 500 μs after the spark.

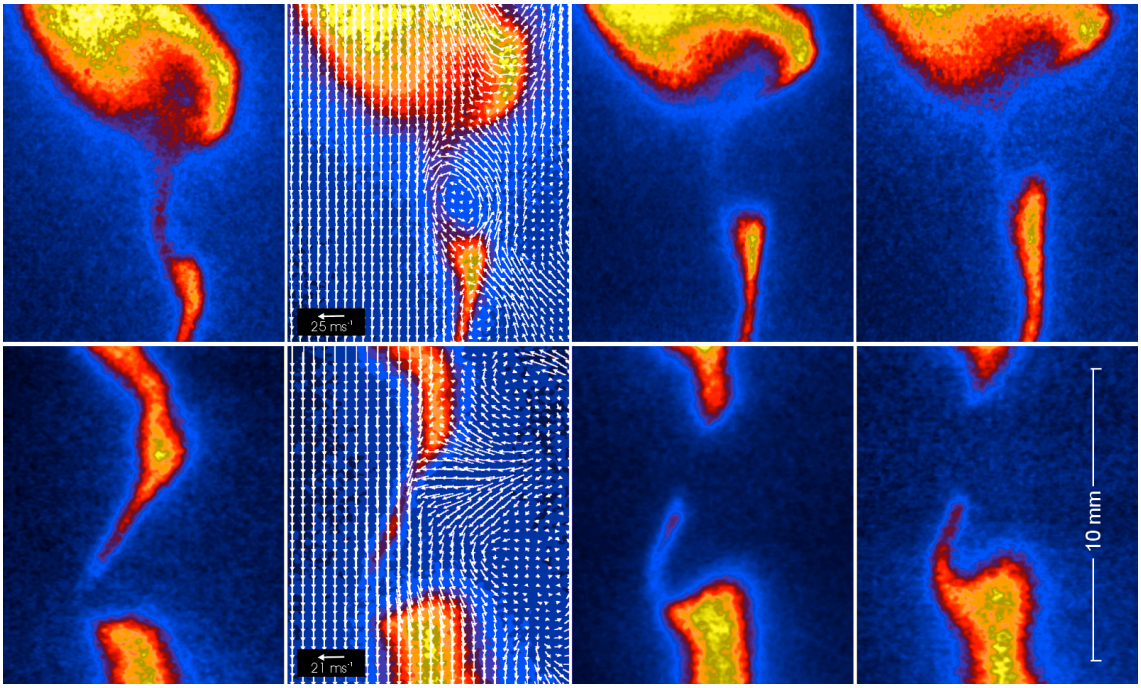

Figure 8: Flame vortex interactions studied by simultaneous application of high speed PLIF imaging of OH and PIV (see main text for details).

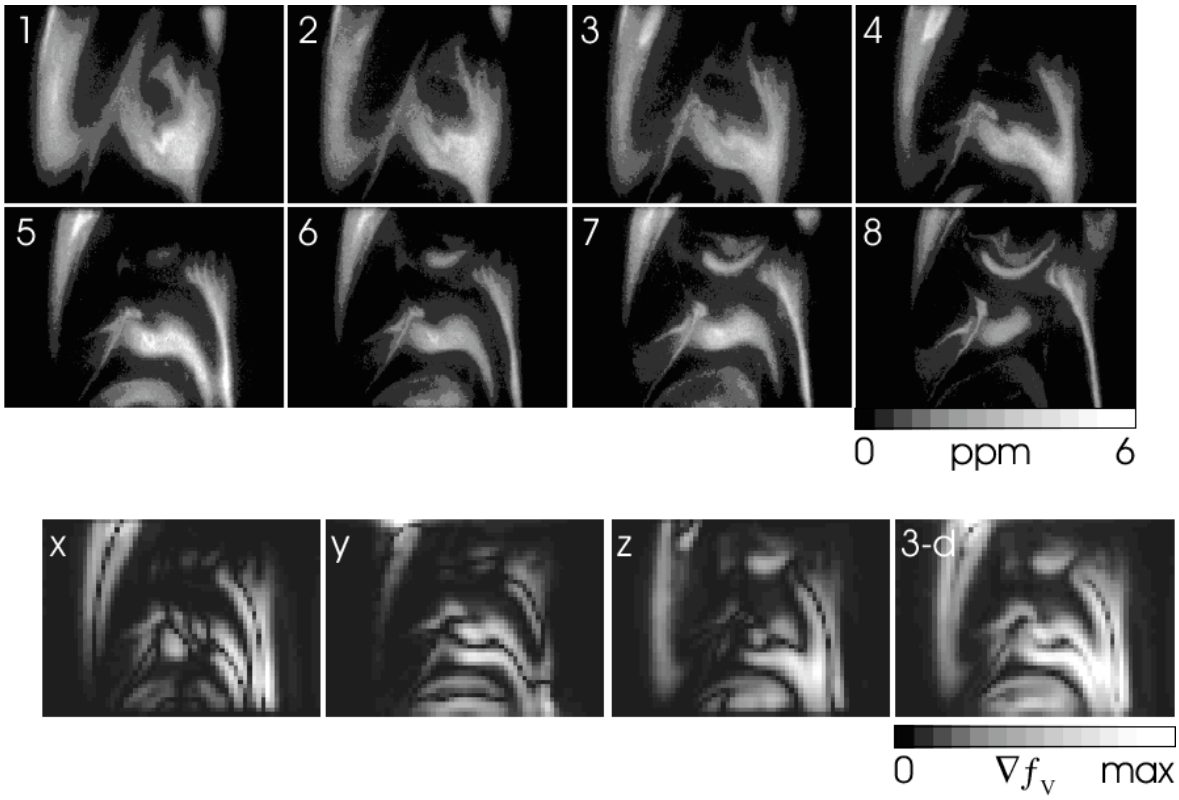

Figure 9: 3D imaging of soot volume fraction in a turbulent ethelene/N_2/air diffusion flame (*Re*=2200, fuel exit velocity 15 ms^{-1}). The images were obtained by rapid slicing of the using a 2D LII technique (21 □ 15 mm image region, time separation 12.5 □s between consecutive images). Soot volume fractions were calibrated on an absolute scale using laminar reference flames. The lower sequence shows concentration gradients along the three cartesian axes from which a true 3D gradient can be reconstructed (last image).

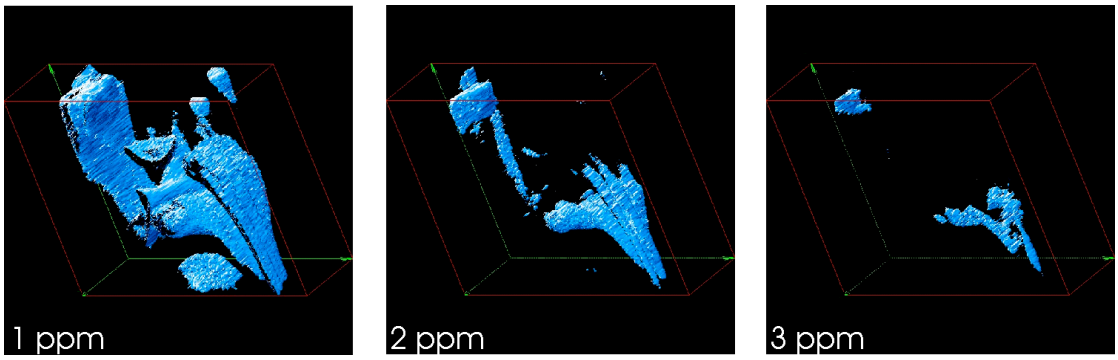

Figure 10: Iso-concentration surfaces reconstructed from the data shown in Fig.11 for three different soot volume fraction levels.